AIP | Journal of Applied Physics

Photovoltaic infrared detection with p-type graded barrier heterostructures

P. K. D. D. P. Pitigala, S. G. Matsik, A. G. U. Perera, S. P. Khanna, L. H. Li et al.

Citation: J. Appl. Phys. **111**, 084505 (2012); doi: 10.1063/1.4704695

View online: http://dx.doi.org/10.1063/1.4704695

View Table of Contents: http://jap.aip.org/resource/1/JAPIAU/v111/i8

Published by the American Institute of Physics.

JOURNAL OF APPLIED PHYSICS **111**, 084505 (2012)

Photovoltaic infrared detection with p-type graded barrier heterostructures

P. K. D. D. P. Pitigala,[1] S. G. Matsik,[1] A. G. U. Perera,[1,a)] S. P. Khanna,[2] L. H. Li,[2]
E. H. Linfield,[2] Z. R. Wasilewski,[3] M. Buchanan,[3] and H. C. Liu[3,b)]
[1]*Department of Physics and Astronomy, Georgia State University, Atlanta, Georgia 30303, USA*
[2]*School of Electronic and Electrical Engineering, University of Leeds, Leeds LS2 9JT, United Kingdom*
[3]*Institute for Microstructural Sciences, National Research Council, Ottawa K1A 0R6, Canada*

(Received 17 November 2011; accepted 16 March 2012; published online 19 April 2012)

Photovoltaic infrared detectors have significant advantages over photoconductive detectors due to zero bias operation, requiring low power and having reduced low frequency noise. They also exhibit no thermally assisted tunneling currents, leading to higher operating temperatures. p-type emitter/graded barrier GaAs/$Al_xGa_{1-x}As$ structures were tested as photovoltaic detectors in the infrared region, operating under uncooled conditions and without an applied bias voltage. A photovoltaic responsivity of 450 mV/W was obtained with a detectivity (D*) of 1.2×10^6 Jones at a peak wavelength 1.8 μm at 300 K. Responsivity and D* increased to $\sim$1.2 V/W and 2.8×10^6 Jones, respectively, at 280 K. A non-linear improvement in responsivity was observed with increased emitter thickness. © *2012 American Institute of Physics*. [http://dx.doi.org/10.1063/1.4704695]

I. INTRODUCTION

Group III–V semiconductor materials are extremely important for the development of infrared (IR) detectors operating over a wide wavelength range.[1–4] Most photovoltaic devices are based on p-n junction structures. Use of superlattice structures for infrared photovoltaic devices has gained increasing interest in recent years.[5–7] Photovoltaic response has been demonstrated in multi-quantum-well structures, which generate a photovoltage owing to the Schottky junction characteristics.[8] Furthermore, photovoltaic multi-quantum-well IR detectors with GaAs/AlGaAs superlattice structures, consisting of n-doped GaAs and undoped AlGaAs layers with a graded barrier at one contact end have also been reported at low temperatures.[9,10] Here, we demonstrate p-doped GaAs/$Al_xGa_{1-x}As$, emitter/graded barrier structures with different aluminum fractions (x), operating as photovoltaic detector under uncooled condition. The zero bias reduces the Joule heating in the device and will also reduce low frequency noise and dark current.

II. PROCEDURE

Six wafers were tested, each consisting of a single barrier/emitter/barrier structure between two contact layers; a schematic of the valence band structure is shown in Fig. 1(a). Of these six wafers, five had the barriers graded with a decreasing Al fraction (X2) from the emitter end and to (X1) towards the bottom contact end of the structure. The sixth sample had a flat barrier instead of the graded barrier as the control sample. All wafers had a constant barrier (X3) between the emitter and the top contact. Device parameters are given in Table I, where X1, X2, and X3 represent the aluminum fractions of the barriers at the bottom contact end and the emitter end of the graded barrier, and in the flat barrier, respectively. Out of the five wafers, three of the graded barriers were grown using continuous alloy fraction variation (SP 1005, SP 1006, SP 1007), whilst the other two (V0727, V0728) were formed by digital alloying as described elswhere.[11]

The sample has a constant barrier ($Al_{0.75}Ga_{0.25}As$) on the bottom contact side (instead of the graded barrier) and a small constant barrier ($Al_{0.57}Ga_{0.43}As$) at the top contact side, separated by a single GaAs emitter layer. The emitters were p-doped to 1×10^{19} cm^{-3} in all six wafers. All wafers studied were grown by molecular beam epitaxy and processed into mesas by wet etching followed by deposition of metal contacts. The photoconductive mode response (response with applied bias) of some of these devices (V0727, V0728) is reported elsewhere.[11]

III. RESULTS

Four dominant photoexcitation and carrier transport mechanism under photovoltaic mode are summarized in Fig. 1(a), using the valence band diagram for the graded barrier structures. In the first path, named h1, the exited carriers (holes) in the bottom contact region scatter from the graded barrier and fall back into the bottom contact layer. In the second path (h2), exited carriers have sufficient energy to overcome the higher end of the graded barrier and are collected at the bottom contact layer even after scattering off the graded barrier. Therefore, a net charge will be accumulated at the bottom contact. This carrier accumulation generates a shift in the energy levels between the two layers (bottom contact and emitter). In the third and fourth paths, h3 and h4, respectively, exited carriers from the emitter (top contact) will pass over the constant barrier and transport to the top contact (emitter) region. The net carrier accumulation at either emitter or top contact will be zero. Therefore, there will be no energy band shift between the top contact and emitter region due to carrier transport between them. Owing to the asymmetry of these carrier transport mechanisms, a photovoltage (V_{ph}) will be generated between the bottom and top contact. For example, a photovoltage of 0.6 mV was

---

[a)] Author to whom correspondence should be addressed. Electronic mail: uperera@gsu.edu. Tel.: 404-413-6037. Fax: 404-413-6025.

[b)] Present address: Department of Physics, Shanghai Jiao Tong University, Shanghai 200240, China.

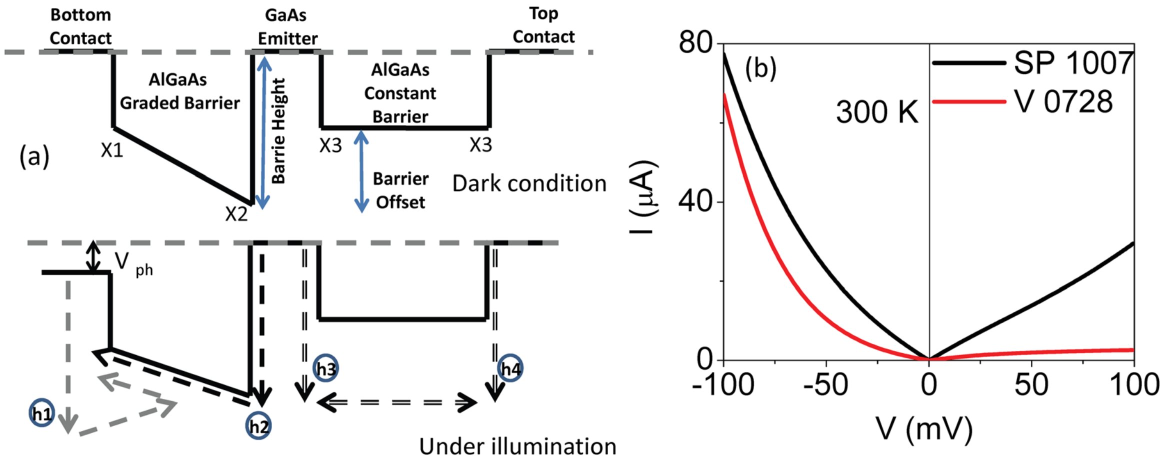

FIG. 1. (a) Schematic diagram of the valence band alignment in the graded barrier structure before (upper) and after (lower) illumination. X1, X2, and X3 represent the aluminum fractions at the two edges of the graded barrier and in the flat barrier (see Table I). Carrier transport processes in the structure are illustrated by arrows. When the device is illuminated, exited carriers (holes) will diffuse over the barriers as represented by arrow paths h1, h2, h3, and h4. The transitions h1 and h2 will result in carrier accumulation at the bottom contact. This generates a shift in the Fermi energy between the two contacts, resulting in a photovoltage (V_{ph}). (b) IV characteristic curve of the devices V0728 and SP1007 at 300 K. Positive or negative bias intend positive or negative voltage applied at the top contact with respect to the bottom contact, respectively.

observed in V0728, when illuminated with the full spectrum of the IR source (1 μm to 5 μm) of an FTIR spectrometer. This response was linearly proportional to the light intensity.

The I–V characteristics for V0728 and SP1007 at 300 K at low bias are shown in the Fig. 1(b). The V0728 has the higher resistance (15 KΩ at zero Bias) and lower dark current compared to SP1007 (2.1 KΩ at Zero Bias) throughout the voltage domain. The asymmetry in the I–V is due to the asymmetry in the device structure. The differences in the barrier heights are causing the differences in resistance for the two devices. At negative bias (top contact negative), the slope of the graded barrier becomes less steep; hence the effective barrier height is reduced allowing an increased dark current to flow through the device. Due to the higher resistance, the carrier accumulation in the V0728 will be higher allowing a large photovoltage buildup compared to the SP1007.

A photovoltaic response was observed for all the tested devices with a graded barrier (V0727, V0728, SP1005, SP1006, and SP1007) showed at room temperature. As the spectral measurements, open circuit voltage of the device was measured by a voltage amplifier (Stanford Research, SR 560) and a Perkin Elmer system 2000 FTIR. The data were calibrated using responsivity of a bolometer. Out of the tested devices, the highest signal was observed for the device from the wafer V0728, as expected through the analysis of I–V data. The open circuit voltage responsivity spectra of a device from this wafer at 280 K and 300 K are shown in Fig. 2(a). At 300 K, a peak responsivity of 460 mV/W was observed at the wavelength of 1.8 μm and the estimated photocurrent is $\sim$ 40 μA/W. The Johnson noise limited specific detectivity value for the device is calculated as $\sim 1.5 \times 10^6$ Jones using

$$D^* = R_v \sqrt{\frac{A}{4kTR_0}}. \tag{1}$$

Here, R_v is the responsivity in volts per watt and, R_0 is the resistance at zero bias, A is the area of the device, k is the Boltzmann constant, and T is the temperature. When the temperature of the device was reduced, an increase in the responsivity and D* to 1.28 V/W and 2.8×10^6 Jones was observed, respectively. A summary of the peak responsivity and D* values at 300 K, at 1.8 μm, is tabulated in Table I. The quantum efficiency (QE) of the devices is calculated to be 0.03% at the peak response.

The responsivity spectra of SP1005, SP1006, and SP1007 at room temperature are shown in Fig. 2(b). SP1007, having a thicker emitter of 80 nm, shows a higher responsivity compared to the other two wafers (SP1006 and SP1005) which have thinner emitters of 50 nm and 20 nm, respectively.

TABLE I. Summary of the device parameters, where X1, X2, and X3 represents the aluminum (Al) fraction of the barriers at the bottom contact and the emitter ends of the graded barrier, and at the constant barrier, respectively. The responsivity and specific detectivity (D*) of the devices at 300 K, and a wavelength of 1.8 μm, are also shown.

Device No.	X1	X2	X3	Emitter thickness (nm)	Peak responsivity (mV/W) at 300 K	D* (Jones) at 300 K
V0727	0.55	1.0	0.57	20	17.1	6.0×10^4
V0728	0.55	1.0	0.57	80	450	1.2×10^6
SP1001	0.75	0.75	0.57	80	—	—
SP1005	0.45	0.75	0.57	20	1.1	9.9×10^3
SP1006	0.45	0.75	0.57	50	3.9	3.3×10^4
SP1007	0.45	0.75	0.57	80	20.8	1.4×10^5

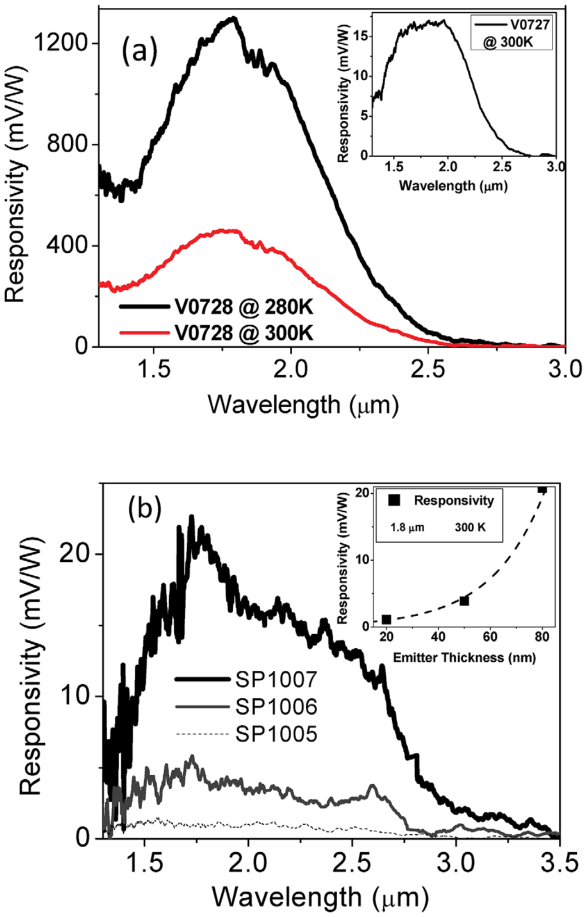

FIG. 2. (a) The photovoltaic response of V0728 at 280 K and 300 K; the photovoltaic response shows a peak at a wavelength of 1.8 μm and a threshold at 2.6 μm. The photovoltaic responsivity increases with the decreasing temperature. Inset: Responsivity of wafer V0727 at 300 K. The responsivity of V0727 is lower owing to the smaller emitter, 20 nm compared to 80 nm in V0728. (b) The photovoltaic response of SP1007, SP1006, and SP1005 at 300 K. The photovoltaic response decreased with decreasing emitter thicknesses (80 nm, 50 nm, and 20 nm, respectively). A peak response was seen at a wavelength of 1.8 μm, and a threshold was observed at 3.5 μm. Inset: The peak responsivity (at 1.8 μm) extracted from response curves of the three devices shows an exponential increase in the responsivity with increasing emitter thickness.

A similar behavior was observed for V0728 and V0727 (responsivity shown in inset of Fig. 2(a)); the response is higher in V0728 with an 80 nm emitter. Since each wafer has the same doping density in the emitter, the device with a thicker emitter is thus likely to have an increased charge accumulation. The higher photovoltage is a result of a higher number of carriers accumulated in the contact region. Wafer SP1001, which did not have a graded barrier, did not show a photovoltaic response when operated close to room temperatures. Without the graded barrier, there will be no net carrier transport in either direction, and hence no photovoltage should be observed.

The ratio of the peak responsivity (1.8 μm) for V0728 to V0727 is ~26, whilst for SP1007 to SP 1005 it is ~19. This responsivity increment is much greater than the ratio in emitter thickness. The responsivity increase in the SP devices with emitter thickness is shown in the inset of Fig. 2(b) and is showing an exponential behavior. This phenomenon has not yet been fully understood. The difference in the responsivity ratios between V07 and SP wafers may, however, be a result of the differences in the rate of scattering at the barriers, owing both to the two different methods used in growth and also to the difference in the aluminum fractions in the graded barriers (the gradient in the barrier). Additionally due to the differences in the device resistance, the accumulated carriers may discharge quickly in the SP series devices compared to the V07 series.

Devices V0728 and V0727 shows a photoresponse threshold at ~2.6 ± 0.2 μm, while SP1005, SP1006, and SP1007 show a broader response region with a threshold around 3.5 ± 0.2 μm. The Arrhenius plot of dark current versus temperature gives the barrier height as ~490 ± 15 meV (2.55 ± 0.1 μm) and ~360 ± 10 meV (3.44 ± 0.1 μm) in agreement with the photovoltaic response threshold. The barrier height calculated using the Anderson rule, conduction band to valance band ratio (CB:VB) of 60:40 gives a VB barrier height ~610 meV for AlAs/GaAs interface in V07 series (barrier due to difference in aluminum fractions $x = 1$ and $x = 0$) and a barrier height of ~430 meV for $Al_{0.75}Ga_{0.25}As$/GaAs interface ($x = 0.75$ and $x = 0$) in the SP series. The constant barrier height is ~300 meV ($x = 0.57$ and $x = 0$) for both the sets of devices. Therefore, the barrier offset for V07 and SP samples is ~310 meV ($x = 0.57$ and $x = 1$) and ~130 meV ($x = 0.57$ and $x = 0.75$), respectively. None of the barrier heights calculated by the Arrhenius data are equivalent to any of the barriers or barrier offsets calculated by the Anderson Rule. The difference in the values obtained by Arrhenius data and Anderson rule can be due to the tunneling effects through thinner region of the graded barrier. Another reason can be the Anderson rule of CB:VB ratio of 60:40 may not be valid for aluminum fraction, $x > 0.45$, as the X-valley becomes lower than the Γ-valley for AlGaAs under this condition and the band gap becomes indirect and lower than the energy difference between VB and Γ-valley.[12] Additionally, CB:VB ratios from 55:45 to 65:35 can be found in literature for GaAs/AlGaAs interface, and 67:32 (66:34) ratio gives the band offset of 488 meV (365 meV) for V07 (SP) devices in agreement with the values calculated by Arrhenius data (490 ± 15 meV and ~360 ± 10 meV).

The variation in D* for V0728 with wavelength in both the photoconductive mode (with a bias of −0.1 V) and photovoltaic mode (0 V bias) is shown in the Fig. 3. The noise generated by the measuring instruments is negligible compared to the device noise. The inset of Fig. 3 shows the noise current density (S(f)) of V0728 at a −0.1V bias voltage and at 0 V bias. At high frequency ($f > 10$ kHz), the measured noise density is closer to the Johnson noise limit. D* calculated with the measured noise at 10 kHz is 1.2×10^6 Jones. As a comparison between the photovoltaic and photoconductive modes of operation, sample V0728 was then operated in photoconductive mode under the negative bias (bottom contact positive) for which it was designed. The D* value of 1.5×10^6 Jones for photovoltaic operation was significantly higher than the photoconductive value of 3.5×10^4 Jones. This indicates the potential for better performances of devices, in the photovoltaic mode of operation using graded barriers at room temperature.

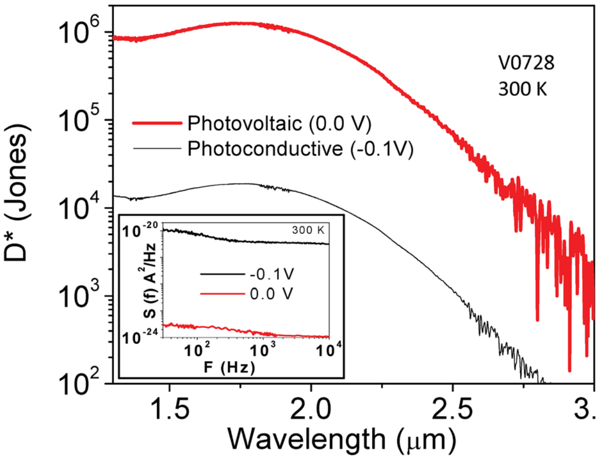

FIG. 3. Detectivity of V0728 as a function of wavelength in a photoconductive mode (with a bias of −0.1V) and photovoltaic mode (0 V bias) at 300 K. Photovoltaic mode has a higher detectivity due to low noise. Inset: The noise current density (S(f)) of V0728 at −0.1 V bias voltage, and 0 V bias, shows a low noise level in the device with 0 V bias due to the absence of shot noise caused by dark current in biased device.

IV. DISCUSSION

The D* obtained for this device is comparatively low compared to other infrared directors working at room temperature and responding in shorter wavelength ($< 2\ \mu$m), such as the p-i-n InGaAs detector with D* of the order of 10^{11} Jones. However, these results shown in this paper are not from a device designed for optimized photovoltaic mode operation. However unlike other detectors, graded barrier detectors are intra-band devices, providing wavelength tunability by adjusting the barrier height. Therefore, implementation of the design can lead to uncooled IR detectors for long wavelength detection. Further improvements to the D* is possible by modifying the structure parameters of the graded barrier device; such as having thicker emitters, adjusting the barrier thicknesses, the aluminum composition in the barriers, multiple layers, emitter doping, and substituting the emitter layer with different materials with higher absorption coefficient. Possible modifications and expected improvement factors summarized in Table II and are briefly discussed below.

Based on the results and calculations published elsewhere,[13] increasing the emitter doping from 1×10^{19} cm^3 up to 3×10^{19} cm^3, an improvement factor of ~3 is expected by increasing the number of excited carriers. Similarly, analyzing the improvement in the responsivity with increasing gradient in the barrier, shown in Figs. 2(a) and 2(b), an improvement by factor of ~3 is expected by lowering the aluminum fractions from X1 = 0.55 to 0.05 at the lower end of the barrier. Lowering the aluminum fraction at the lower end of the graded barrier will allow the VB in the bottom contact to shift further, generating a higher response voltage. And with addition of 30 emitter/barrier layers will improve the photon absorption; hence an improvement factor of 25 is expected. Multilayer structure will increase the photon absorption in the device; hence more carriers will be excited and accumulated in the contact region. Additionally, multilayer device can act as a series connection of individual units, therefore increase the response voltage. Furthermore, keeping the resistance of the device to an optimum value by adjusting the barrier thicknesses, that maintains the low noise as well as a high responsivity, will improve the D* by an additional factor of 3 or more improving the D* to about 10^9 Jones, make this device competitive with the reported photovoltaic devices operates under low applied bias voltage.[14] Additionally an improvement factor of ~15 can be expected via enhancing the absorption using surface plasmon effects; theoretical models have predictions of around 20 times enhancement of absorption via plasmon effects.[15,16] The result is a total enhancement with a factor of 10^4. Furthermore by adopting different materials with high absorption coefficient (α; at $\lambda \sim 1\ \mu$m, T ~295 K and p-doped) than GaAs ($\alpha \sim 20\,\text{cm}^{-1}$)[17] such as InN ($\alpha \sim 10^3\ \text{cm}^{-1}$)[18] and InP ($\alpha \sim 200\,\text{cm}^{-1}$)[19] shall enhance the absorption, hence the performance of the device by a factor of 10 or more. This offers the prospect of the detectivity to be greater than 10^{11} Jones which is a competitive with commercially available detectors, such as the p-i-n InGaAs detector with D* of the order of 10^{11} Jones.

V. CONCLUSION

In conclusion, single emitter barrier structures with p-doped GaAs emitters and undoped AlGaAs graded barriers were tested for their photovoltaic response. We found that structures with a graded barrier had a photovoltaic response at room temperature and without any applied bias voltage. A device with a higher aluminum fraction in the graded barrier (x = 1 to 0.55), and with an emitter thickness of 80 nm, showed the highest responsivity of ~450 mV/W at 300 K. This responsivity was shown to increase as temperature decreased. Furthermore, increasing the emitter region thickness by a factor of four led to an increase in the peak responsivity by factor of ~26. Devices also showed better D* values when operated in a photovoltaic mode rather than in a

TABLE II. Summary of expected enhancement factors due to modifications proposed for the present structure.

Description	Present value	Proposed value	Expected improvement factor in D*
Increase doping	1×10^{19} cm^{-3}	3×10^{19} cm^{-3}	3
Gradient in the barrier (X1)	0.55	0.05	3
Number of layers (30)	1	30	25
Impedance (Johnson noise)	15 kΩ	2 kΩ	3
Plasmon effect	—	15	15
High absorbing material	GaAs ($\alpha \sim 20$ cm^{-1})	InN ($\alpha \sim 10^3$ cm^{-1})	50
		InP ($\alpha \sim 200$ cm^{-1})	10

photoconductive mode. Possibility of further enhancing the responsivity and detectivity is discussed. Additionally, the concepts presented in this paper can be extended to long wavelength IR radiation in the 8–14 μm range, as well as the terahertz frequency range, using phosphide and nitride based materials. Use of a photovoltaic mode of operation thus offers considerable potential advantages for long wavelength detection.

ACKNOWLEDGMENTS

This material is based upon work supported by, or in part by, the U.S. Army Research Laboratory and the U. S. Army Research Office under Contract/Grant No. W911NF-08-1-0448. We also acknowledge support from the EPSRC (UK) and the European Research Council program "TOSCA." Additionally, we wish to thank Dr. Y.F. Lao for his valuable comments.

[1] P. V. V. Jayaweera, S. G. Matsik, A. G. U. Perera, H. C. Liu, M. Buchanan, and Z. R. Wasilewski, Appl. Phys. Lett. **93**(2), 021105–021103 (2008).

[2] A. Weerasekara, M. Rinzan, S. Matsik, A. G. Perera, M. Buchanan, H. C. Liu, G. von Winckel, A. Stintz, and S. Krishna, Opt. Lett. **32**(10), 1335–1337 (2007).

[3] Y. F. Lao, P. K. D. D. P. Pitigala, A. G. U. Perera, H. C. Liu, M. Buchanan, Z. R. Wasilewski, K. K. Choi, and P. Wijewarnasuriya, Appl. Phys. Lett. **97**(9), 091104–091103 (2010).

[4] D. G. Esaev, M. B. M. Rinzan, S. G. Matsik, and A. G. U. Perera, J. Appl. Phys. **96**(8), 4588–4597 (2004).

[5] D. L. Smith and C. Mailhiot, J. Appl. Phys. **62**(6), 2545–2548 (1987).

[6] H. Mohseni, A. Tahraoui, J. Wojkowski, M. Razeghi, G. J. Brown, W. C. Mitchel, and Y. S. Park, Appl. Phys. Lett. **77**(11), 1572–1574 (2000).

[7] A. Rogalski and P. Martyniuk, Infrared Phys. Technol. **48**(1), 39–52 (2006).

[8] C. S. Wu, C. P. Wen, R. N. Sato, M. Hu, C. W. Tu, J. Zhang, L. D. Flesner, L. Pham, and P. S. Nayer, IEEE Trans. Electron Devices **39**(2), 234–241 (1992).

[9] A. Kastalsky, T. Duffield, S. J. Allen, and J. Harbison, Appl. Phys. Lett. **52**(16), 1320–1322 (1988).

[10] K. M. S. V. Bandara, J.-W. Choe, M. H. Francombe, A. G. U. Perera, and Y. F. Lin, Appl. Phys. Lett. **60**(24), 3022–3024 (1992).

[11] A. G. U. Perera, S. G. Matsik, D. P. Pitigala, Y. F. Lao, S. P. Khanna, L. H. Li, E. H. Linfield, Z. R. Wasilewski, M. Buchanan, X. H. Wu, and H. C. Liu, Infrared Phys. Technol. **54**(3), 296–301 (2011).

[12] W. Yi, V. Narayanamurti, H. Lu, M. A. Scarpulla, and A. C. Gossard, Phys. Rev. B **81**(23), 235325 (2010).

[13] S. G. Matsik, P. V. V. Jayaweera, A. G. U. Perera, K. K. Choi, and P. Wijewarnasuriya, J. Appl. Phys. **106**(6), 064503–064506 (2009).

[14] E. Plis, S. Annamalai, K. T. Posani, S. J. Lee, and S. Krishna, Proc. SPIE **6206**(1), 62060O (2006).

[15] C. Daboo, M. J. Baird, H. P. Hughes, N. Apsley, and M. T. Emeny, Thin Solid Films **201**(1), 9–27 (1991).

[16] M. S. Shishodia, P. V. V. Jayaweera, S. G. Matsik, A. G. U. Perera, H. C. Liu, and M. Buchanan, Photonics Nanostruct. –Fundam. Appl. **9**(1), 95–100 (2011).

[17] J. H. C. Casey, D. D. Sell, and K. W. Wecht, J. Appl. Phys. **46**(1), 250–257 (1975).

[18] J. Trainor and K. Rose, J. Electron. Mater. **3**(4), 821–828 (1974).

[19] H. Burkhard, H. W. Dinges, and E. Kuphal, J. Appl. Phys. **53**(1), 655–662 (1982).